IEEE Access
Multidisciplinary ⋮ Rapid Review ⋮ Open Access Journal

Received September 16, 2020, accepted October 18, 2020, date of publication October 21, 2020, date of current version November 2, 2020.

*Digital Object Identifier 10.1109/ACCESS.2020.3032747*

# 3D Spherical Panoramic Epipolar Line Based on Essential Matrix

**SHUAI LIU[1,2], JUN CHEN[2], MIN SUN[3], LINGLI ZHAO[1], XIANG WEI[1], AND HONGWEI GUO[1], (Member, IEEE)**

[1]College of Engineering, Honghe University, Mengzi 661100, China
[2]National Geomatics Center of China, Beijing 100048, China
[3]Institute of Geographic Information Systems and Remote Sensing, Peking University, Beijing 100871, China

Corresponding author: Lingli Zhao (zll_csu@126.com)

This work was supported in part by the National Natural Science Foundation of China under Grant 41761079; in part by the Universities Joint Special Foundation of Yunnan Provincial Science and Technology Department in China under Grant 2018FH001-046, Grant 2018FH001-056, and Grant 2017FH001-06; in part by the Key Projects of the Universities Joint Special Foundation of Yunnan Provincial Science and Technology Department in China "Study on the Estimation Method of Pomegranate Yield Based on Machine Learning Geometric Feature Panoramic Image Pattern Recognition;" in part by the Young and Middle-Aged Academic and Technical Leader Reserve Project of Yunnan Province in China under Grant 201905AC160009; and in part by the Top Young Talent Project of Yunnan Province in China.

**ABSTRACT** A 3D spherical panoramic epipolar line based on essential matrix is proposed in this study to solve the search range to improve calculation efficiency and reliability of the matching. First, this method uses the essential matrix of computer vision principles to establish the epipolar geometry model of spherical panoramic image. Second, it derives the epipolar line mathematical equations and characteristics of spherical panoramas. Third, it calculates statistics on the distribution law of epipolar images. Experimental results show that the feasibility of the method proposed in this study. The proposed method effectively verified the trajectory of the spherical panoramic epipolar line, finished distribution of epipolar line sequence trajectory and decreased the search range of the corresponding points. The findings help lay a solid foundation for the matching and measurement of the panoramic measurement model and the generation of depth maps.

**INDEX TERMS** Spherical panoramas, epipolar line, essential matrix.

## I. INTRODUCTION

The epipolar constraint can reduce the image matching search space from two dimensions to one, thereby improving computational efficiency and reliability. Current research work and applications of epipolar lines are mainly based on pinhole central projection with a limited field of view (FOV), resulting in various problems such as image blind spots and insufficient overlaps. Panorama brings a 360° full FOV landscape but has specific geometric modeling and projection transformations. The construction of epipolar line constraints is a key issue in the field of computer vision and close-range digital photogrammetry.

A spherical stereovision system based on the double fish-eye lens has been proposed. This system can expand the FOV to 190° and expand the epipolar lines into parallel ones, to which the search range of points with the same name is limited. Thus, the search efficiency is improved.

The associate editor coordinating the review of this manuscript and approving it for publication was Huazhu Fu.

The scalability of a panorama has captured research attention in recent years. Luhmann [14] derived a cylindrical panoramic epipolar line model; Fangi [15]–[17] provided the spherical panoramic epipolar line equation from photogrammetry; Li *et al.* [18] deduced the mathematical equation of the panoramic epipolar line based on the hyperbolic and parabolic characteristics; Zhengpeng *et al.* [19] presented the epipolar line distribution of the vehicle-mounted cubic panoramic image and constructed constraints to achieve matching gross error detection; Fanyang *et al.* [20] used vehicle GPS/IMU(Global Positioning System/Inertial Measurement Unit) and other information to derive panoramic epipolar images, established geometric constraints on epipolar lines between panoramic images, and eliminated mismatching; Svoboda and Pajdla [21] determined the geometric features of spherical panoramic epipolar lines as large circles; Torrii *et al.* [22] used the geometric duality characteristics of points and large circles to derive the epipolar constraints of two and three panoramic images. However, the above works need to meet certain constraints, such as optical flow [19]

and precise attitude [20], or only theoretically derive the panoramic epipolar line [15]–[17], [21]–[22]. Thus, studies on the verification and practical applications of panoramic epipolar line are lacking. The feature of epipolar constraint that can improve reliability, accuracy, and speed of panoramic image matching has not been fully applied to the 3D information processing of panoramic images.

Therefore, this study carries out an in-depth analysis of the projection geometry of spherical panoramic images, uses the essential matrix of computer vision principles to establish the epipolar geometry model of such image, derives its mathematical equations and characteristics, and calculates statistics on the distribution law of epipolar images. The analysis provides a theoretical basis for the application of epipolar lines in spherical panoramic images. Experiments prove that the spherical panoramic epipolar equation is correct and feasible. Comparison shows that the proposed method is more versatile than the photogrammetric method, which requires certain initial conditions to derive the geometric relationship of the epipolar line.

## II. ESTABLISHMENT OF THE DOUBLE SPHERICAL PROJECTION GEOMETRIC RELATIONSHIP

Computer vision and photogrammetry theory are used in establishing the relationship between two projection planes and their corresponding points to realize the 3D position of a projection point. On a panoramic image, the 3D position of a target point on a panoramic image is determined by developing a similar geometric relationship, called a double spherical projection geometric relationship. A single panorama constructed via photography cannot solve the measurement problem; thus, this study introduces the concept of stereo panorama. That is, two panoramas are captured at different locations in the same place and constructed to solve the measurement problem.

Fangi [15]–[17] established a coplanar formula between two spherical panoramas. However, this formula is essentially consistent with traditional photogrammetry, which does not use spherical geometric characteristics and can only solve unknown trace values. That is, this formula requires an initial value to solve the problem, causing inconvenience in outdoor data acquisition.

### A. GEOMETRIC MODELING OF THE PANORAMIC MODEL

A spherical panoramic image is designed to provide users with 360° full-view landscape view and observation. The essential component is a sphere model with an observation point at the center. A multi-view scene with a sequence of images is related to the sphere surface through certain mapping, forming a visual with 360° seamless observation of the scene.

The mapping relation between point $P'$ on the sphere and point $p'$ on the panoramic image can be constructed [15]–[17]. Formulas (1) and (2) present the corresponding relations between the spherical angle parameters $(\varphi, \theta)$ of the pixel coordinates $p\ (x,\ y)$ on the image plane and the 3D point coordinates $P\ (X,\ Y,\ Z)$, respectively.

$$\begin{cases} x = R \cdot \phi \\ y = R \cdot \theta \\ R = a/2\pi \end{cases} \tag{1}$$

$$\begin{cases} X = R \cdot \sin\phi \cdot \sin\theta \\ Y = R \cdot \cos\phi \cdot \sin\theta \\ Z = R \cdot \cos\theta \end{cases} \tag{2}$$

Suppose $\rho = \sqrt{X_P^2 + Y_P^2 + Z_P^2}$, then the relationship between points $P$ and $p$ can be expressed as

$$\begin{aligned} m &= \left[\, R\sin\theta\cos\varphi \;\; R\sin\theta\sin\varphi \;\; R\cos\theta \,\right]^T \\ &= \frac{R}{\rho}\left[\, X_p \;\; Y_p \;\; Z_p \,\right]^T \end{aligned} \tag{3}$$

Suppose $\lambda = \frac{R}{\rho}$, therefore $m = \lambda M_p$. The coordinates of point $P$ and of its projection points differ by only one scaling factor. When all points are projected onto the unit sphere, that is, set $R = 1$, then

$$m = \left[\, \sin\theta\cos\varphi \;\; \sin\theta\sin\varphi \;\; \cos\theta \,\right]^{\mathrm{T}} \tag{4}$$

## III. DERIVATION OF THE EPIPOLAR EQUATION OF SPHERICAL PANORAMIC IMAGE

### A. GEOMETRIC DEFINITION OF EPIPOLAR LINES

In computer multi-view geometry and photogrammetry, the geometric relationship between the two images is commonly expressed by a coplanar equation or by an epipolar line relationship. For spherical projection, the epipolar line is no longer a straight line but two spherical great circle curves. See Corollary 1, as shown in Figure 1.

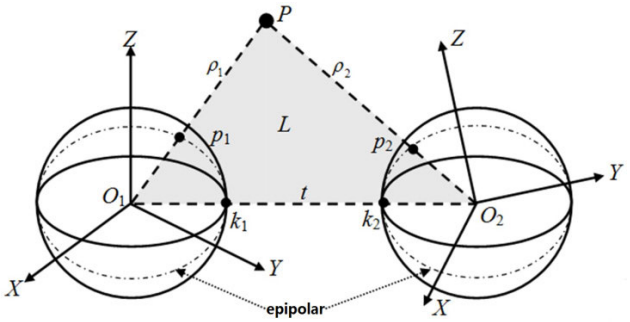


**FIGURE 1.** Double spherical projective geometry.

*Corollary 1:* Trajectory of the epipolar line of the spherical panoramic image is the great circle of the spherical panoramic sphere

*Proof:* The epipolar geometry is the intersection of plane L formed by the point P, baseline $O_1O_2$, and the image plane. In a spherical panorama, epipolar geometry does not intersect the image plane but rather the spherical surface, as shown in Figure 1. The two arcs $p_1k_1$ and $p_2k_2$ are the epipolar lines of the two spherical panoramic images.

According to the definition of epipolar geometry, plane $L$ passes through the centers of spheres $O_1$ and $O_2$, where the intersection of plane $L$ and the spherical panoramic sphere also passes through.

The intersection of plane L and the spherical panoramic sphere should be the spherical panoramic great circle centered on point $O_1$ and the sphere center $O_2$, respectively.

Therefore, the epipolar lines $p_1k_1$ and $p_2k_2$ are respectively an arc on the great circle of two different spherical panoramic spherical surfaces. This proves that the epipolar track of the spherical panoramic image is a completed great spherical circle curve.

Suppose the coordinates of the space point $P$ in the two spherical projection coordinate systems are $\boldsymbol{M_1}$ and $\boldsymbol{M_2}$, the two corresponding projection points are $p_1$ and $p_2$, and their coordinates are $m_1$ and $m_2$, respectively. One of the spherical projection systems can obtain another system through the rotation matrix $R$ and the translation matrix $\boldsymbol{t}$. Therefore, $\{\boldsymbol{M}_1, \boldsymbol{t}, \boldsymbol{RM}_2+\boldsymbol{t}\}$ is coplanar, and thus

$$\boldsymbol{M}_1^T(\boldsymbol{t} \times (\boldsymbol{RM}_2 + \boldsymbol{t})) = 0 \tag{5}$$

Suppose $\boldsymbol{E} = [\boldsymbol{t}]_\times \boldsymbol{R}$, then

$$\boldsymbol{M}_1^T \boldsymbol{E} \boldsymbol{M}_2 = 0 \tag{6}$$

According to the calculation principle of multi-view geometry [26], $E$ is the essential matrix. According to Formula (3), we can obtain

$$\boldsymbol{m}_1^T \boldsymbol{E} \boldsymbol{m}_2 = 0 \tag{7}$$

When $\boldsymbol{m}_1$ is known, suppose $\boldsymbol{m}_1^T \boldsymbol{E} = [a\ b\ c]$, $a$, $b$, and $c$ are the vector components (that is, the parameters in Equation (8)), and the coordinate $\boldsymbol{m_2}$ of $\boldsymbol{p_2}$ is $\left[ sin\theta_2 cos\varphi_2 \ sin\theta_2 sin\varphi_2 \ cos\theta_2 \right]$ from Equation (7), we obtain

$$a \sin\theta_2 \cos\varphi_2 + b \sin\theta_2 \sin\varphi_2 + c \cos\theta_2 = 0 \tag{8}$$

Therefore, when the coordinate $\boldsymbol{m_1}$ of $p_1$ is known, as long as $E$ is calculated, the trajectory of the epipolar line passing through $p_2$ can be determined.

### B. MATHEMATICAL MODEL OF EPIPOLAR LINE

Assuming that the coordinate of $a$ point in the reference image is $(x_0, y_0)$, the mathematical model of its corresponding epipolar line is deduced as follows.

Step 1. Use a matching algorithm to match two panoramic images, and perform coordinate conversion on the extracted corresponding feature points.

The feature points are extracted and matched by matching algorithm on two panoramic images, and the pixel coordinates of feature corresponding points are converted into spherical projection coordinates according to Formulas (1) (4).

Step 2. Use the 8-point method [26] to find the essential matrix $E$.

The coordinates of the corresponding points taken are normalized and transformed, and the transformed coordinates are respectively set as $(x_i, y_i, 1)$ and $\left(x_i', y_i', 1\right)$, where $i = 1, 2, \cdots, n$. Substitute the normalized coordinates of the points into the following matrix $A$.

$$\boldsymbol{A} = \begin{bmatrix} x_1'x_1 & x_1'y_1 & x_1' & y_1'x_1 & y_1'y_1 & y_1' & x_1 & y_1 & 1 \\ \vdots & \vdots & \vdots & \vdots & \vdots & \vdots & \vdots & \vdots & \vdots \\ x_n'x_n & x_n'y_n & x_n' & y_n'x_n & y_n'y_n & y_n' & x_n & y_n & 1 \end{bmatrix} \tag{9}$$

Perform SVD decomposition on A and de-normalize to obtain $E$.

Step 3. Find the parameters $[a, b, c]$ according to the obtained essential matrix and determine the epipolar line trajectory equation.

According to Formula (8), the epipolar line trajectory equation can be converted to

$$\begin{cases} \left(\dfrac{a}{c} \cdot \sin\varphi_2 + \dfrac{b}{c} \cdot \cos\varphi_2\right) \cdot \sin\theta_2 + \cos\theta_2 = 0, & c \neq 0 \\ a \sin\theta_2 \cos\varphi_2 + b \sin\theta_2 \sin\varphi_2 = 0, & c = 0 \end{cases} \tag{10}$$

Then

$$\begin{cases} \theta_2 = \arctan\left(-\dfrac{1}{\dfrac{a}{c} \cdot \sin\varphi_2 + \dfrac{b}{c} \cdot \cos\varphi_2}\right), & c \neq 0 \\ \varphi_2 = \arctan\left(-\dfrac{a}{b}\right), & c = 0 \end{cases} \tag{11}$$

Equation (11) is the trajectory equation formed by the corresponding epipolar line in the virtual sphere on the right. This equation takes $\varphi_2$ as the parameter and value range is $0$–$2\pi$.

The coefficients $a$, $b$, and $c$ can be obtained according to the coordinates of the known reference sphere points and the calculated essential matrix E. Equation (11) constitutes the relationship between $\varphi_2$ and $\theta_2$. When $c \neq 0$, with $\varphi_2$ as the parameter, the value range is $0$–$2\pi$ and the value of $\theta_2$ can be determined by $\varphi_2$. When $c = 0$, $\varphi_2$ is a certain value, that is, the epipolar line is perpendicular to the X-axis.

Step 4. Use Ransac algorithm to eliminate matching gross errors and iteratively calculate the essential matrix $E$.

According to the epipolar line trajectory determined by $E$, the epipolar line constraint relationship is established and the gross error of the matching pair is eliminated. The Ransac algorithm is used to repeatedly execute Steps 2–3, eliminate matching gross errors, iteratively calculate the essential matrix E, and output the final epipolar trajectory Formula (11).

### C. EPIPOLAR MATHEMATICAL MODEL OF CLOSE-RANGE PHOTOGRAMMETRY

Section B derives the mathematical geometric equation of the panoramic epipolar line based on the essential matrix of the computer vision principle. By comparison, this section establishes the geometric model of the panoramic image epipolar line of the close-range photogrammetry method based on the coplanar equation to verify the method proposed in this

study. The fourth part experimentally compares the geometric equations of epipolar lines obtained by the two methods.

In Figure 3, suppose $O_1$ and $O_2$ are the projection centers of two adjacent spherical panoramas, respectively, and the value of the baseline $O_1O_2$ is $B\,(b_x\ b_x u b_x v)^T$, and the rotation parameter of the right spherical panoramic sphere relative to the left spherical panoramic sphere is ($\Phi$, $\Omega$, $K$).

**Step 1: Solve the coordinates of points$O_1$, $O_2$, and $p_2$in the spherical panoramic sphere coordinate system on the right.**

Let the coordinates of the center $O_1$ of the left spherical panoramic sphere be $(0\ 0\ 0)^T$. The value of the baseline $O_1O_2$ is $B$. Therefore, the coordinate of $O_2$ point in the left spherical panoramic coordinate system is $(b_x\ b_x u b_x v)^T$. The three points of points $p$, $O_1$ and $O_2$ are translated, rotated, and converted to the spherical panoramic sphere coordinate system on the right. The coordinates of the three points in the new reference system can be obtained. Given that the value of the baseline $O_1O_2$ is $B(b_x b_x u\ b_x v)^T$, the rotation parameter is ($\Phi$, $\Omega$, $K$). The rotation matrix R from the spherical panoramic coordinates on the left to the spherical panoramic coordinates on the right is (12), as shown at the bottom of the page.

Assuming that the coordinates of any point Q in the spherical panoramic coordinate system on the left are $\begin{pmatrix} X & Y & Z \end{pmatrix}^T$, the coordinates of the spherical panoramic coordinate system on the right are:

$$\begin{pmatrix} X_{new} \\ Y_{new} \\ Z_{new} \end{pmatrix} = R \cdot \begin{pmatrix} X - b_x \\ Y - b_x \cdot \mu \\ Z - b_x \cdot v \end{pmatrix} \tag{13}$$

Point $O_2$ is the origin of the spherical panoramic sphere on the right and its coordinates are:

$$\begin{pmatrix} X_{O_2} & Y_{O_2} & Z_{O_2} \end{pmatrix}^T = \begin{pmatrix} 0\ 0\ 0 \end{pmatrix}^T \tag{14}$$

The coordinates of point C1 in the spherical panoramic sphere coordinate system on the right are:

$$\begin{pmatrix} X_{O_1} \\ Y_{O_1} \\ Z_{O_1} \end{pmatrix} = R_2 \cdot \begin{pmatrix} 0 - b_x \\ 0 - b_x \cdot \mu \\ 0 - b_x \cdot v \end{pmatrix} = -b_x \cdot R_2 \cdot \begin{pmatrix} 1 \\ \mu \\ v \end{pmatrix} \tag{15}$$

The coordinates of point $P'$ are:

$$\begin{pmatrix} X_P \\ Y_P \\ Z_P \end{pmatrix} = R_2 \cdot \begin{pmatrix} X' - b_x \\ Y' - b_x \cdot \mu \\ Z' - b_x \cdot v \end{pmatrix} \tag{16}$$

wherein $(X'Y'Z')$ is obtained by Formulas (1) and (2).

**Step 2: Find the equations of the plane where points $O_1$, $O_2$, and p are located.**

Suppose the general equation of the epipolar surface $L$ is:

$$AX + BY + CZ + D = 0 \tag{17}$$

Given that the epipolar surface $L$ passes through points $p$, $O_1$, and $O_2$, substituting the coordinates of the three points into Formula (17) can obtain the equation of core surface $L$:

$$\begin{cases} a_1 = -\dfrac{1}{X_{O_1}} \cdot \left(a_2 \cdot Y_{O_1} + Z_{O_1}\right) \\ a_2 = \dfrac{X_{O_1} \cdot Z_P - X_P \cdot Z_{O_1}}{X_P \cdot Y_{O_1} - X_{O_1} \cdot Y_P} \\ a_1 \cdot X + a_2 \cdot Y + Z = 0 \end{cases} \tag{18}$$

$a_1$ and $a_2$ are the coefficients of the epipolar surface $L$ equation.

**Step 3: Solve the trajectory equation of the epipolar line.**

The spherical equation on the right $X''^2 + Y''^2 + Z''^2 = R^2$ is a function of the parameters $\theta''$ and $\varphi''$ in the polar coordinate system.

$$\begin{cases} X'' = R \cdot \sin\theta'' \cdot \sin\phi'' \\ Y'' = R \cdot \cos\theta'' \cdot \sin\phi'' \\ Z'' = R \cdot \cos\phi'' \end{cases} \tag{19}$$

The epipolar line to be sought should be the intersection of the epipolar surface L and the right sphere. Therefore, substituting Formula (19) into Formula (18) and subtracting $R$ from the left and right of the equation, we obtain:

$$\left(a_1 \cdot \sin\theta'' + a_2 \cdot \cos\theta''\right) \cdot \sin\phi'' + \cos\phi'' = 0 \tag{20}$$

By subtracting $cos\ \varphi''$ from the equation, we obtain

$$\phi'' = \arctan\left(-\frac{1}{a_1 \cdot \sin\theta'' + a_2 \cdot \cos\theta''}\right) \tag{21}$$

The trajectory equation formed by the corresponding epipolar line in the virtual sphere on the right is Formula (21), which takes $\theta''$ as the parameter and the value range is 0– $2\pi$. Substituting the left spherical center point $O_1(X_{O_1} Y_{O_1} X_{O_1})^T$ and point $p\ (Xp\ Yp\ Zp)^T$ into Formula (18), $a_1$ and $a_2$ can be obtained. Equation (21) constitutes the relationship between $\theta''$ and $\varphi''$. The equation assumes $\theta''$ as a parameter and the value range is 0–$2\pi$. The value of $\varphi''$ can be determined by $\theta''$.

## IV. EXPERIMENT AND RESULT ANALYSIS

### A. EXPERIMENTAL DESIGN

This section verifies the points projected on the panorama and counts their considerable circle trajectories; in addition, due to the possibility of various errors in the stitching and parameter calculation of the panorama image, the corresponding points are not strictly located on the corresponding epipolar lines.

$$R = inv(R_1) = inv\left(\begin{pmatrix} \cos\Phi & 0 & -\sin\Phi \\ 0 & 1 & 0 \\ \sin\Phi & 0 & \cos\Phi \end{pmatrix} \cdot \begin{pmatrix} 1 & 0 & 0 \\ 0 & \cos\Omega & -\sin\Omega \\ 0 & \sin\Omega & \cos\Omega \end{pmatrix} \cdot \begin{pmatrix} \cos K & -\sin K & 0 \\ \sin K & \cos K & 0 \\ 0 & 0 & 1 \end{pmatrix}\right) \tag{12}$$

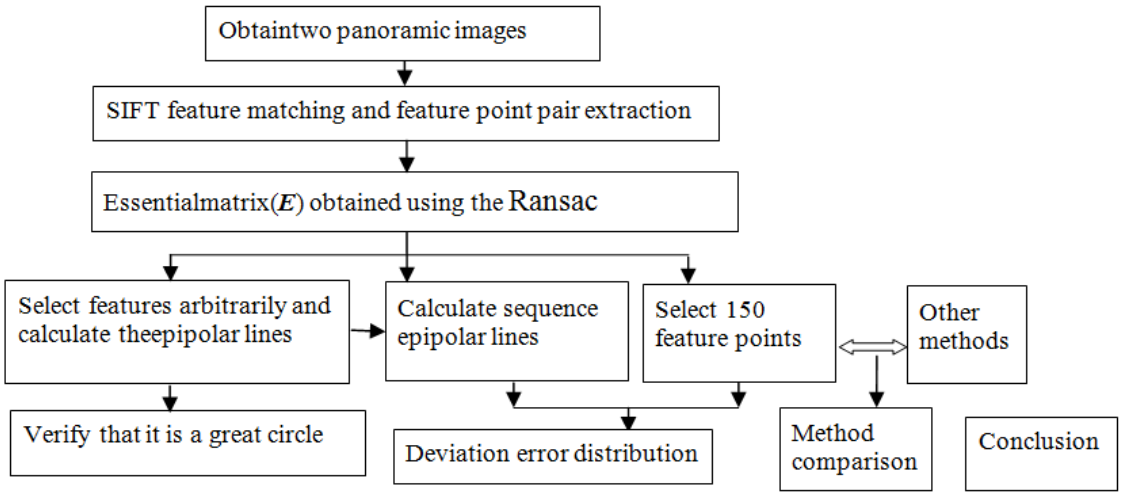


**FIGURE 2.** Experimental design flow chart.

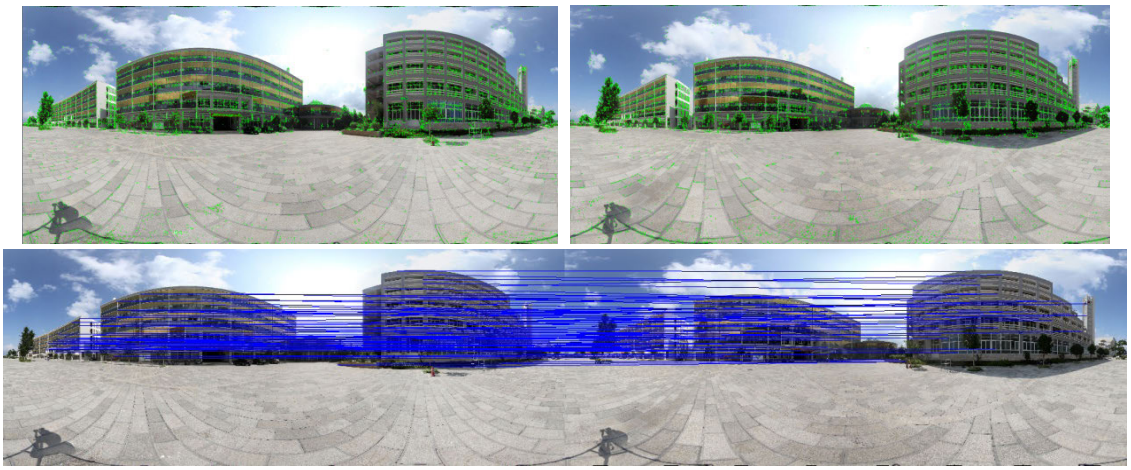

**FIGURE 3.** Result of matching two panoramic images using the SIFT method.

In this study, the experiments are designed and verified for these two aspects: 1) Verification of the trajectory of the spherical panoramic epipolar line; 2) Calculate the deviation degree of the corresponding epipolar line, analyze the images projected by multiple sets of epipolar lines on the panoramic image, and obtain the influence of the epipolar line constraint on the deviation degree of the feature point matching search range; 3) The generation method and deviation of the epipolar constraint are given, and the method is compared with others.

Shooting experiments are conducted outside a building by using the camera model Canon EOS 5D Mark with fish-eye lens (Canon EF8-15mm). The camera head was JTS-Rotator SPH. An ordinary tripod and central leveling are also used. Six photographs are shot at each position every 60°, and the photographs are then spliced into two spherical panoramic images by using commercial software, as shown in Figure 3. The photographs are used as an example to verify the algorithm proposed in this work. Station spacing is approximately 7 m and arranged at two sides of the orientation control device (red circle in Figure x). One of the panoramic images is selected as the reference image. Figure 2 illustrates the experimental design.

### *B. EXPERIMENTAL VERIFICATION*

The relative orientation algorithm of traditional photogrammetry involves determining the pixel coordinates of the image plane that corresponds to more than five points in the two panoramic images and solving the parameters of the relative position and attitude relationship of the two photographs.

#### 1) FEATURE EXTRACTION MATCHING AND EPIPOLAR LINE GENERATION

According to the experimental design shown in Figure 2, the scale-invariant feature transform (SIFT) algorithm is used to match two panoramic images. As shown in Figure 4, 101 pairs

(a) Select two feature points (b) Epipolar track diagram

**FIGURE 4.** Schematic diagram of the trajectory of epipolar points.

of matches and 34 pairs of mismatches are found. The Ransac algorithm is used to compute the essential matrix $E$.

Select two feature points from the reference image as shown in Figure 4a, and calculate the trajectories of their epipolar lines according to Formula (11), which is all a closed curve as shown in Figure 4b.

### 2) EPIPOLAR LINE GREAT CIRCLE VERIFICATION

According to the theory of spherical panoramic imaging, a complete epipolar line mapped to the spherical panoramic coordinate system should be a large circle with a radius of 636.6 pixels (the width of the panoramic image is 4000 pixels, $4000/2\pi$ =636.6), which can be inversely calculated. To verify the epipolar line, we take point Q from the epipolar line (the black point in Figure 5a), and the symmetrical point (the red point in Figure 5a) that is 180° apart can be calculated. Then calculate whether the pixel distance between Q and is equal to twice the radius. For any epipolar line, 100 points can be taken, two points with a difference of 180° are a group (as shown in Figure 5b, the collinear black and red points), a total of 50 points. Calculate the distance converted to each group of points on the sphere (such as the collinear black dots and red dots in Figure 5c) and verify whether they are all twice the radius, that is, the epipolar line is considered to be a large arc.

According to Formula (11), it can be divided into two cases, $C \neq 0$ and $C = 0$, and the second case is special. This experiment mainly proves the first case. Arbitrarily pick a point in the reference panoramic image, and the corresponding epipolar line in the right image is calculated by Formula (11), where $\theta$ is a parameter with a value range of 0–$2\pi$, and the value of $\varphi$ can be determined by $\theta$. Given that the *arctan* function has a value range between $[-\pi\ /\ 2, +\pi\ /\ 2]$, Formula (1) states that the point in the panorama can correspond to values within the range of $[0, \pi]$. Thus, the value of $\varphi$ should be mapped to $[0, \pi]$ interval. When $\varphi < 0$, $\varphi = \pi + \varphi$. Assuming that the coordinate angle of point $q$ on the epipolar line is $(\theta_0, \varphi_0)$, the coordinate angle of the corresponding point of the spherical center that is 180° apart is:

$$\begin{cases} \theta' = \begin{cases} \pi + \theta_0 & \theta_0 \in [0, \pi) \\ \theta_0 - \pi & \theta_0 \in [\pi, 2\pi) \end{cases} \\ \phi' = \pi - \phi_0 \end{cases} \tag{22}$$

According to Formulas (1) and (4), the coordinates and distances of the corresponding spatial points (the black point in Figure 5(a)) and (the red point in Figure 5(a)) can be obtained. As shown in Figures 5(b) and 5(c), the diameter error calculated by selecting 50 sets of points are all within 0.001 pixel. This computation can confirm that the epipolar line is imaged as a large arc with a radius of 636.6 pixels.

### 3) DEVIATION OF THE EPIPOLAR LINE

To count the deviation degree of the corresponding epipolar lines, the reference panoramic image is divided into 200 regions according to the size of 200 $*$ 200 pixels. Figure 6 shows that every two black dividing lines form a region, some of which have no feature correspondence. Therefore, 125 feature points are taken from 42 areas, numbered 1–125 from left to right, and the red cross hair represents the selected feature points.

Theoretically, the point must be on its corresponding epipolar line. However, as shown in Figure 4, deviations occur in actual applications due to image collection and stitching, extraction of feature points, number and distribution of corresponding points, and errors caused by the orientation.

In the following, statistics are computed on the degree of deviation of the aforementioned 125 feature corresponding

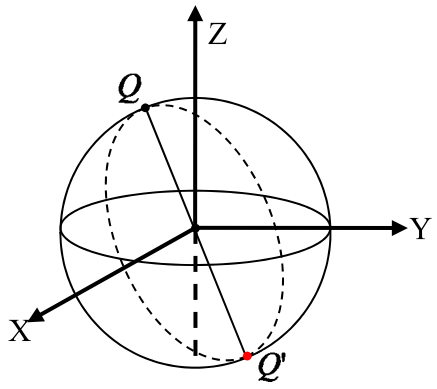


(a) Three-dimensional epipolar line

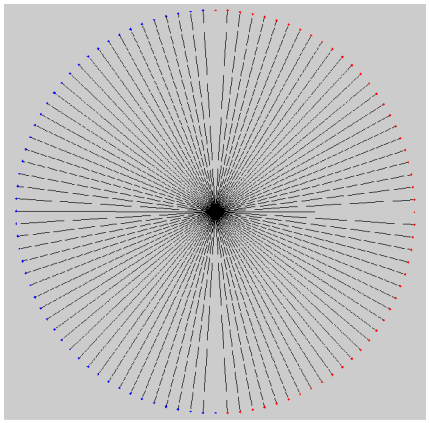

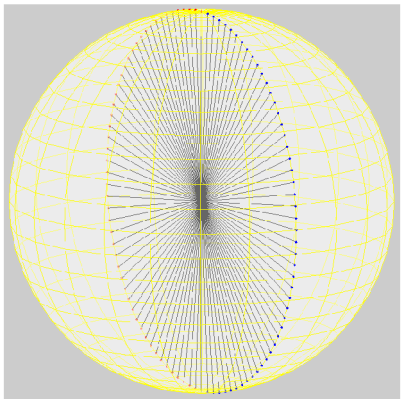

(c) Epipolar grouping in three-dimensional space

**FIGURE 5.** Schematic diagram of spherical panoramic epipolar line trajectory verification.

points and their epicenter distances. Figure 7 shows this specific situation. The percentage of points deviating from over 30 pixels is 13%, and that of points within 30 pixels is 87%. The points with large deviations are distributed near the baseline.

#### 4) DISTRIBUTION OF EPIPOLAR LINE SEQUENCE TRAJECTORY

To further analyze the reason why the epipolar line is located near the baseline and exhibits considerable deviation, we conduct a series of epipolar line trajectory generation experiments. Select a series of points in the reference image to maintain the same abscissa of pixels, and the ordinates are separated by a certain number of pixels (if the number of pixels is small, then the generated epipolar line sequence is dense; otherwise, the epipolar line sequence is sparse. This study uses 100 pixels) and then add one set of epipolar line sequence in another image as shown by the blue line in Figure 8(b). A total of 40 epipolar lines in the two groups also intersect at two epipolar points. From this analysis, all epipolar lines can be deduced to intersect at two epipolar points.

As the distance of the epipolar lines to the baseline (the connecting line between the two epipolar points) decreases, the density of the epipolar lines increases. Therefore, the greater the deviation of the epipolar line from the corresponding point, the greater the measurement error. Thus, the measurement near the baseline is even more difficult to perform effectively.

#### 5) EPIPOLAR LINE ASSISTED MATCHING SEARCH

Given the errors, the corresponding points are not necessarily located on the epipolar line. The statistical results of the deviation show that over 80% of the corresponding points are located within 30 pixels near the epipolar line. Therefore, the corresponding point matching search and the search area (between the two blue lines) can be opened up along the epipolar track (red line) as shown in Figure 9. Feature points are quickly matched near the red line to improve search efficiency.

#### 6) COMPARISON AND DEVIATION ANALYSIS OF PANORAMIC EPIPOLAR LINE GENERATION METHODS

Both the close-range photogrammetry method and the computer vision method are used to determine the epipolar line geometric relationship by constructing the coplanar equation to obtain the coefficient parameters. The coefficients of the two can be converted to each other, and the epipolar line trajectory is similar or essentially the same. Table 1 shows the differences.

In the current panoramic epipolar line generation method, photogrammetry commonly uses the beam adjustment or the least squares, while computer vision mainly uses the RANSAC algorithm. The former typically requires more constraints, such as camera calibration [14]–[18]. The vehicle-mounted cubic panoramic method requires constraints such as optical flow [19] and position and attitude information [20]. The degree of epipolar deviation has not been studied and analyzed in greater detail. Section III (D) derives the spherical panoramic epipolar line by constructing the close-range photogrammetric coplanar equation to verify the proposed method, as shown in Figure 10. The blue line group is the epipolar line series of the method in Section III (D), and the red line group is the epipolar line series of the proposed method. Therefore, the degree of deviation of the epipolar line is close to that in the proposed

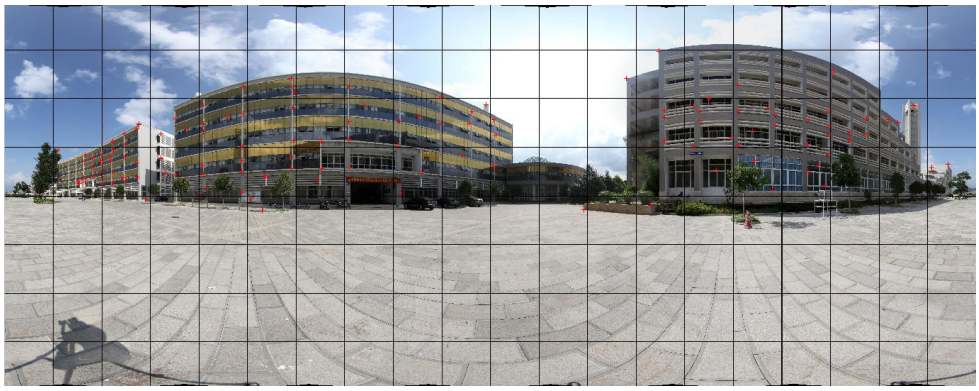

**FIGURE 6.** Schematic regional division and feature point distribution.

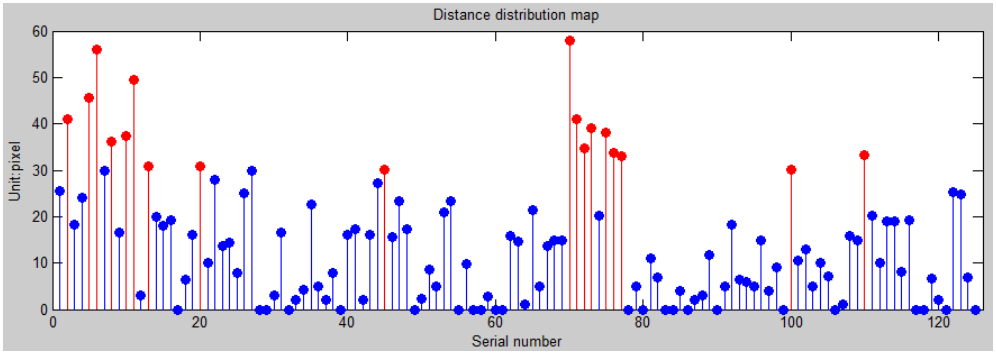


**FIGURE 7.** Error map of the corresponding points deviating from the epipolar line.

**TABLE 1.** Panoramic core line production method and its deviation comparison.

| | Calculation strategy | Initial constraints | Degree of epipolar line deviation |
|---|---|---|---|
| Traditional close-range photogrammetry method [14-18] | Beam adjustment | Precise camera calibration and image correction, etc. | Not yet evaluated |
| Vehicle-mounted cubic panoramic hybrid method [19-20] | RANSAC algorithm[19], Least squares method [20] | Optical flow [19], position and posture information [20], etc. | Not yet evaluated |
| The close-range photogrammetry method (Section3.3) | Least squares method | The initial angles of the two base stations are the same | Deviation of more than 30 pixels accounted for 12.8%, deviation of less than 30 pixels accounted for 87.2% |
| Method of this article | RANSAC algorithm | No initial conditions required | Deviation of more than 30 pixels accounted for 14.4%, deviation of less than 30 pixels accounted for 85.6% |

method. Furthermore, the proposed method does not require initial constraints. Experiment 6) uses the initial angle difference to deviate the images of the two methods and their epipolar lines, which verifies that the method in this paper is more versatile.

### 7) INFLUENCE OF INITIAL ANGLE DIFFERENCE ON PARAMETER CALCULATION AND COMPARISON

The effect of the initial angle difference on the proposed method and close-range photogrammetry was verified. The initial angle difference is the difference in the initial angle direction of the panoramic image. Figure 11 shows that the panoramic images a and c were acquired at Station 1 while b was acquired at Station 2. Images a and b have the same initial angles, which differ from that of Image c. In this experiment, the difference in initial angle is approximately 15°. The six panoramas are captured at different locations, as shown in Figure 12.

In this study, the following conclusions are drawn from experiments with multiple sets of different azimuth angles.

(a) First group of epipolar line series

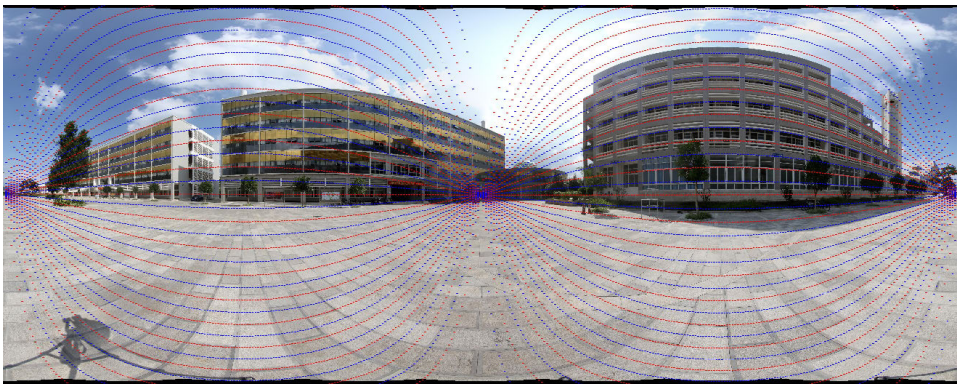

(b) Second group of epipolar line series

**FIGURE 8.** Epipolar line series diagram.

**FIGURE 9.** Auxiliary feature matching of panoramic epipolar line.

**TABLE 2.** Comparison of the calculation of the parameters of the two methods with the initial angle difference of about 15°.

| | Data | Initial angle | method | parameters |
|---|---|---|---|---|
| No.1 | Image *a* and image *b* | same | Section III(C) | a = -0.7036 b = 0.0176 c = 0.1003 |
| No.2 | Image *c* and image *b* | different | Section III(C) | a = -0.7024 b = 0.0177 c = 0.1008 |
| No.3 | Image *a* and image *b* | same | Method of this paper | $a_1$ = -3.7289 $a_2$ = -5.8802 |
| No.4 | Image *c* and image *b* | different | Method of this paper | $a_1$ = -2.6690 $a_2$ = -19.8261 |

When the initial angle difference is small, the parameters of the two methods and the distribution of the epipolar line sequence have little effect. Therefore, the following experimental azimuth angles are approximately 15° and the specific experimental parameters of the two types of methods and the deviation of the distribution of the epipolar line sequence are presented. The two sets of data of images a and b, and images c and b in Figure 12 are respectively calculated and compared using the method in Section III (D), as shown in Table 2.

According to the four sets of parameters obtained in Table 2, the epipolar line series trajectories are generated. Figure 13 shows that the epipolar line series trajectories of the

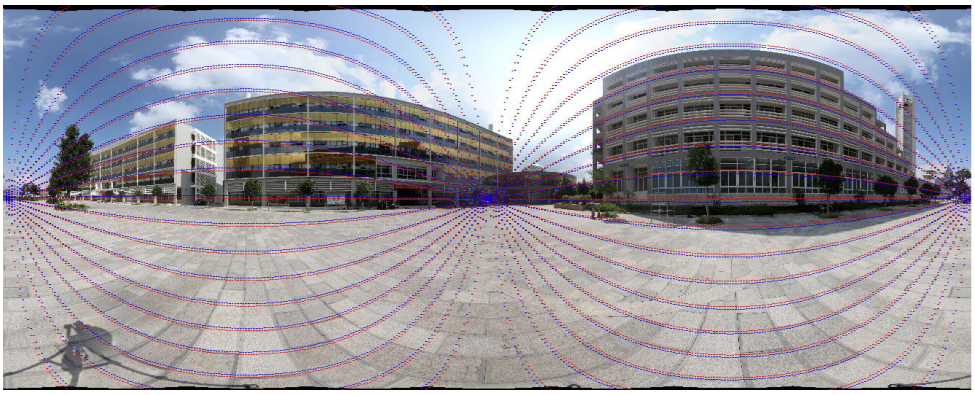

**FIGURE 10.** Comparison diagram of two methods of epipolar line series.

first, third, and fourth groups are similar, and the intersecting pairs of poles are close. The trajectories of the two sets of epipolar lines are uneven, and the intersecting opposite pole positions differ from the other three sets. From this analysis, we can infer that when the two panoramic images have large initial angle differences, the use of close-range photogrammetry may lead to a relation. The instability of the orientation parameter, the offset generated by the epipolar line, and the initial angle difference of the proposed method has little effect and has better versatility. The following conclusions are drawn from the experiments with multiple sets of different azimuth angles: The initial angle difference is 3° within, the distribution of the epipolar line sequence of the two types of methods has a small deviation. As the azimuth angle increases, the impact of the proposed method decreases while that of the Section III (D) method increases, and even the relative orientation cannot be completed. However, how the degree of time affects these two types of methods and how to prove the theory still needs further research, when the initial angle is between 0–360°.

### 8) DEVIATION ANALYSIS

Generally speaking, the factors that affect epipolar deviation primarily include the quality of the camera itself (e.g., resolution and CCD sensor), intersection angle, feature point extraction, and control point selection. Analysis of these factors is summarized as follows: a) Unless a professional measuring camera and its professional calibration settings are used, the errors introduced by camera quality and its internal parameters are the highest in number and are difficult to eliminate. b) The error introduced by feature point extraction and matching generally does not exceed 1 pixel. c) Determining the number of errors introduced during image correction and stitching requires research. d) Selection of control points exhibits a significant relationship with the distribution of points to be measured in a scene. That is, accuracy is high when the control points are close to the orientation reference frame. In general, measurement accuracy along the direction of the baseline vertical centerline is compromised, and taking effective measurements on the spherical surface near the extension of the baseline is difficult. Obtaining accurate measurements with a uniform distribution within the panoramic range remains a problem that requires further research.

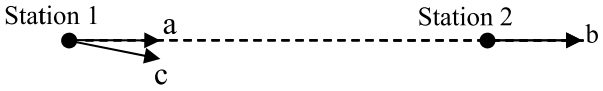


**FIGURE 11.** Schematic diagram of station establishment.

(a) Image a taken at station 1

(b) Image b taken at station 2

(c) Image c taken at station 1

**FIGURE 12.** Experimental images.

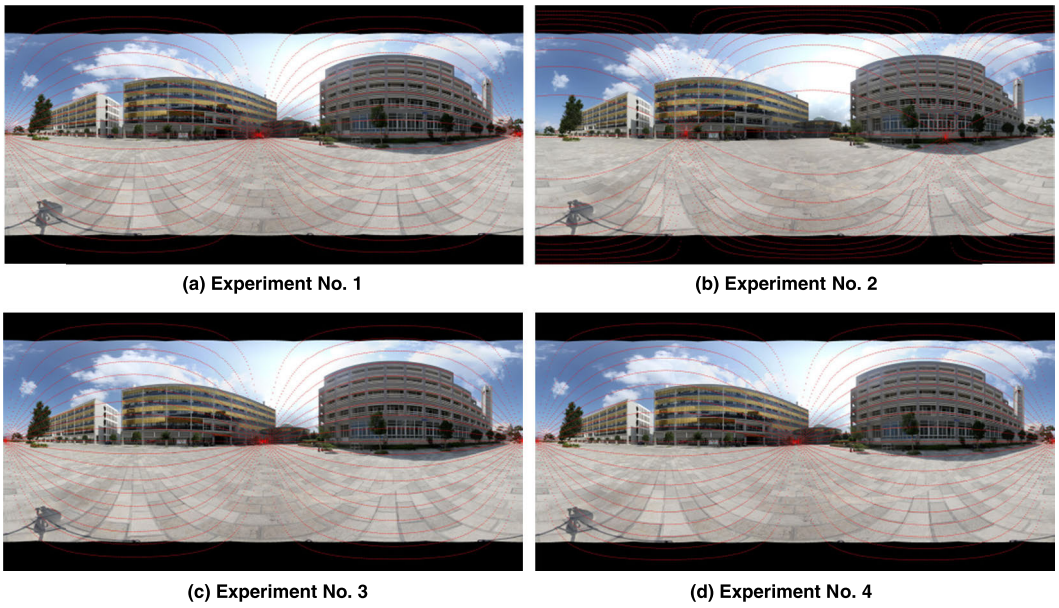

(a) Experiment No. 1 (b) Experiment No. 2

(c) Experiment No. 3 (d) Experiment No. 4

**FIGURE 13.** Four sets of epipolar line series diagrams.

## V. CONCLUSION

This study uses the essential matrix of multi-view geometry to derive the mathematical model of spherical panoramic epipolar lines aiming at the projection geometry of spherical panoramic images. The experiment effectively verifies the great circle feature of the epipolar line, performs error statistics and analysis on the deviation degree of the epipolar line, and compares various panoramic epipolar line methods. All the epipolar lines intersect at the two epipolar points, the deviation error around the epipolar point and the baseline is large, and the error during measurement is large. In theory, the corresponding point must be on the corresponding epipolar line, but due to the existence of various influence errors, the spherical panoramic epipolar line has a certain distance deviation but can still effectively verify the trajectory of the spherical panoramic epipolar line, finish distribution of epipolar line sequence trajectory and decrease the search range of the corresponding points. The findings help lay a solid foundation for the matching and measurement of the panoramic measurement model and the generation of depth maps.

In the future, many aspects of work still require further study: 1) Problem of epipolar line deviation. This study deduces that the spherical projection epipolar line deviation is affected by many factors, such as the feature points in the panoramic image acquisition, stitching and relative orientation, number and distribution of azimuth and azimuth constraints, and how the error is propagated; 2) Image feature matching problem. Panorama brings full-field scene information but has inconsistent features such as geometric projection, rotation transformation, and scaling relationship, which increase in view of the difficulty and complexity of feature matching. The SIFT feature matching algorithm in this study still cannot solve the gross errors caused by the texture redundancy and scale changes of the panoramic image. Further research and construction of a robust panoramic feature matching method remain necessary; 3) Automatic problem of matching algorithm in the second measurement. The spherical panoramic core line constraint reduces the search range to a certain extent. On this basis, examining the corresponding algorithm to achieve automatic matching of feature points during measurement is necessary.

## REFERENCES


[1] K. Zhizhong, Z. Shunyi, and Z. Zuxun, "Epipolar image generation and corresponding point matching based on vehicle-based images along optical axis," *Geomatics Inf. Sci. Wuhan Univ.*, vol. 31, no. 7, p. 582, 2006.

[2] K. Zhizhong, Z. Zuxun, and Y. Fanlin, "Relative orientation and epipolar arrangement based on forward moving image pairs along the optical axis," *Acta Geodaetica et Cartographica Sinica*, vol. 36, no. 1, pp. 56–61, 2007.

[3] Z. Ka, S. Yehua, and Y. Chun, "Digital close-range stereo image matching based on digital parallax model and improved SIFT features," *Acta Geodaetica et Cartographica Sinica*, vol. 39, no. 6, pp. 624–630, 2010.

[4] H. Fen, W. Mi, and L. Deren, "Generation of approximate epipolar images from linear pushbroom satellite stereo-imagery based on projection reference plane," *Acta Geodaetica et Cartographica Sinica*, vol. 38, no. 5, pp. 428–436, 2009.

[5] Z. Yongjun and D. Yazhou, "Approximate epipolar image generation of linear array satellite stereos with rational polynomial coefficients," *Geomatics Inf. Sci. Wuhan Univ.*, vol. 34, no. 9, pp. 1068–1071, 2009.

[6] Y. Xiuxiao and W. Zhenli, "A method of epipolar image generation based on POS data," *Geomatics Inf. Sci. Wuhan Univ.*, vol. 33, no. 6, pp. 560–564, 2008.

[7] S. G. Li and K. Fukumori, "Spherical stereo for the construction of immersive VR environment," *Proc. IEEE Virtual Reality*. Los Alamitos, CA, USA: IEEE Computer Society Press, Jun. 2005, pp. 217–222.

[8] S. Li, "Real-time spherical stereo," in *Proc. 18th Int. Conf. Pattern Recognit. (ICPR)*, 2006, pp. 1046–1049.

[9] S. Li, "Binocular spherical stereo," *IEEE Trans. Intell. Transp. Syst.*, vol. 9, no. 4, pp. 589–600, Dec. 2008.

[10] Q. Chi, L. Qiang, and S. Jiaguang, "Video mosaic for panoramic image," *J. Comput.-Aided Des. Comput. Graph.*, vol. 13, no. 7, pp. 605–609, 2001.
[11] F. Xianyong, P. Zhigeng, and X. Dan, "An improved algorithm for image mosaics," *J. Comput.-Aided Des. Comput. Graph.*, vol. 15, no. 11, pp. 1362–1365, 2003.
[12] M. Brown and D. G. Lowe, "Automatic panoramic image stitching using invariant features," *Int. J. Comput. Vis.*, vol. 74, no. 1, pp. 59–73, Apr. 2007.
[13] J. Amiri Parian and A. Gruen, "Sensor modeling, self-calibration and accuracy testing of panoramic cameras and laser scanners," *ISPRS J. Photogramm. Remote Sens.*, vol. 65, no. 1, pp. 60–76, Jan. 2010.
[14] T. Luhmann, "Panorama photogrammetry for architectural applications," *Mapping*, no. 1, pp. 40–45, 2010.
[15] G. Fangi, "The multi-image spherical panoramas as a tool for architectural survey," in *Proc. 21st Int. CIPA Symp.* Atene, Greece: ISPRS International Archive, 2011, pp. 21–26.
[16] G. Fangi, "Further developments of the spherical photogram-metry for cultural heritage," in *Proc. 22nd CIPA Symp.* Kyoto, Japan: ISPRS International Archive, 2009, pp. 11–15.
[17] G. Fangi, "Multiscale multiresolution spherical photogrammetry with long focal lenses for architectural surveys," *Int. Arch. Photogram., Remote Sens. Spatial Inf. Sci.*, vol. 38, no. 5, pp. 1–6, 2010.
[18] Y. Li, H.-Y. Shum, C.-K. Tang, and R. Szeliski, "Stereo reconstruction from multiperspective panoramas," *IEEE Trans. Pattern Anal. Mach. Intell.*, vol. 26, no. 1, pp. 45–62, Jan. 2004.
[19] Z. Zhengpeng, J. Wanshou, and Z. Jing, "A gross error detection method of vehicle-borne cubic panaramic image sequence," *Geomatics Inf. Sci. Wuhan Univ.*, vol. 39, no. 10, pp. 1208–1213, 2014.
[20] Z. Fanyang, Z. Ruofei, and S. Yang, "Vehicle panoramic image matching based on epipolar geometry and space forward intersection," *J. Remote Sens.*, vol. 18, no. 6, pp. 1230–1236, 2014.
[21] T. Svoboda and T. Pajdla, "Epipolar geometry for central catadioptric cameras," *Int. J. Comput. Vis.*, vol. 49, no. 1, pp. 23–37, 2002.
[22] A. Torii, A. Imiya, and N. Ohnishi, "Two-and three-view geometry for spherical cameras," in *Proc. 6th Workshop Omnidirectional Vis., Camera Netw. Non-Classical Cameras*. Beijing, China: OMDIVIS Workshop Press, 2005, pp. 1–8.
[23] L. Shuai, C. Jun, and S. Min, "A three dimensional measurement approach and experiment based on spherical panorama," *J. Geo-Inf. Sci.*, vol. 16, no. 1, pp. 15–22, 2014.
[24] L. Shuai, C. Jun, S. Min, and Z. Lingli, "Measurable panorama construction based on binocular spherical projective geometry," *J. Comput.-Aided Des. Comput. Graph.*, vol. 27, no. 4, pp. 657–665, 2015.
[25] L. Shuai, C. Jun, and S. Min, "The derivation and application of spherical panoramic epipolar geometry," *J. Geo-Inf. Sci.*, vol. 17, no. 3, pp. 274–280, 2015.
[26] R. Hartley and A. Zisserman, *Multiple View Geometry in Computer Vision*, 2nd ed. Cambridge, U.K.: Cambridge Univ. Press, 2004.
[27] Shaghai Jietu Software Company. *Stitching Software*. Accessed: Sep. 8, 2020. [Online]. Available: http://www.jietusoft.com/products/zaojingshi/
[28] D. G. Lowe, "Distinctive image features from scale-invariant keypoints," *Int. J. Comput. Vis.*, vol. 60, no. 2, pp. 91–110, Nov. 2004.
[29] Z. Zuxun, "Digital photogrammetry and computer vision," *Geomatics Inf. Sci. Wuhan Univ.*, vol. 29, no. 12, pp. 1035–1039, 2004.